The Meteoritical Society

Meteoritics & Planetary Science 44, Nr 8, 1133–1149 (2009)
Abstract available online at http://meteoritics.org

What metal-troilite textures can tell us about post-impact metamorphism in chondrite meteorites

Andrew G. TOMKINS

School of Geosciences, Monash University, Melbourne, Victoria 3800, Australia
*Corresponding author: E-mail: andy.tomkins@sci.monash.edu.au

(Received 14 November 2008; revision accepted 22 June 2009)

Abstract–Metal-troilite textures are examined in metamorphosed and impact-affected ordinary chondrites to examine the response of these phases to rapid changes in temperature. Complexly intergrown metal-troilite textures are shown to form in response to three different impact-related processes. (1) During impacts, immiscible melt emulsions form in response to spatially focused heating. (2) Immediately after impact events, re-equilibration of heterogeneously distributed heat promotes metamorphism adjacent to zones of maximum impact heating. Where temperatures exceed ~850 °C, this post-impact metamorphism results in melting of conjoined metal-troilite grains in chondrites that were previously equilibrated through radiogenic metamorphism. When the resulting Fe-Ni-S melt domains crystallize, a finely intergrown mixture of troilite and metal forms, which can be zoned with kamacite-rich margins and taenite-rich cores. (3) At lower temperatures, post-impact metamorphism can also cause liberation of sulfur from troilite, which migrates into adjacent Fe-Ni metal, allowing formation of troilite and occasionally copper within the metal during cooling. Because impact events cause heating within a small volume, post-impact metamorphism is a short duration event (days to years) compared with radiogenic metamorphism (>10^6 years). The fast kinetics of metal-sulfide reactions allows widespread textural changes in conjoined metal-troilite grains during post-impact metamorphism, whereas the slow rate of silicate reactions causes these to be either unaffected or only partially annealed, except in the largest impact events. Utilizing this knowledge, information can be gleaned as to whether a given meteorite has suffered a post-impact thermal overprint, and some constraints can be placed on the temperatures reached and duration of heating.

INTRODUCTION

The Van Schmus-Wood criteria for classifying chondritic meteorites (Van Schmus and Wood 1967) is the currently accepted means of distinguishing between petrologic types 3 to 6. Each of these petrologic types represents a bracket of metamorphic grade generally thought to correspond to heating of asteroids early in the history of the solar system, caused by decay of short-lived radioactive isotopes, mainly ^{26}Al (e.g., Trieloff et al. 2003), referred to here as radiogenic metamorphism. However, it has been suggested that impact heating may be responsible for textures considered characteristic of higher metamorphic grades in some meteorites (Rubin 2004, 2007).

The peak temperature reached through radiogenic metamorphism within the interior of an asteroid is a critical input parameter in thermal evolution models (e.g., McSween et al. 2002). This peak temperature can be calculated using silicate thermometry on ortho- and clinopyroxene. However, this temperature parameter is only relevant to thermal evolution models if it reflects radiogenic metamorphism, and not the impact heating proposed by Rubin (2004). The two-pyroxene thermometer currently provides the only means of estimating peak metamorphic temperature for petrologic type 6 chondrites (other thermometers are useful at lower metamorphic grades). However, silicate thermometry has some difficulties (reviewed by Slater-Reynolds and McSween 2005). For example, pyroxene pairs in type 6 ordinary chondrites have compositions indicating that complete thermochemical equilibrium is not recorded, which generates considerable error in the estimated temperatures, in many cases exceeding ±50 °C. The plagioclase, olivine-spinel and oxygen isotope thermometers have closure temperatures well below the peak metamorphic conditions of petrologic type 6 (Slater-Reynolds and McSween 2005; Kessel et al. 2007). The experiments used to establish the pyroxene thermometer

involved run times from three days to three weeks for temperatures relevant to petrologic type 6 (Lindsley 1983), indicating that significant re-equilibration between silicates is possible at relatively short time scales under high temperature conditions. These short domestically are thought to be within the duration of heating events associated with large impacts on planetesimals (cf. Monteux et al. 2007), although this is not well constrained for impacts into small porous bodies. Therefore, a way of distinguishing between metamorphism due to radiogenic rather than impact heating needs to be established.

The problem of mineral thermometer closure temperatures is also encountered by metamorphic petrologists studying the evolution of Earth rocks, who have partially circumvented the issue by studying instead the reactions necessary to produce observed mineral textures, for which the required P-T-X conditions have been experimentally determined (e.g., Holland and Powell 1998). In the same way, metal-sulfide textures have the potential to record a minimum metamorphic temperature (either radiogenic or impact related) in chondrites because the assemblage Fe-Ni + FeS melts at conditions that have been well constrained by experimentalists (the exact temperature depending on the Ni/Fe ratio of the metal). Previous studies have used metallographic textures to examine the conditions of radiogenic metamorphism (Reisner and Goldstein 2003), and subsequent cooling (Wood 1967). Scott (1982) specifically examined the formation mechanisms of complex metal-troilite textures in chondrites, and this work has been used and built upon by others (e.g., Bennett and McSween 1996; Rubin 1994, 2004, 2007) to catalog and examine the effects of shock-related metamorphism.

In this study, metal-sulfide textures contained in L6 and H5 chondrites are re-examined to clarify distinction between textures associated with radiogenic metamorphism, impact-induced melting and post-impact metamorphism. It is shown that examination of metal-sulfide textures is the best way to constrain the peak temperature reached within a sample during post-impact metamorphism because these phases respond quickly to short duration temperature fluctuations whereas silicate minerals do not. New constraints are placed on the process of metal-troilite melting and consequent textural evolution during post-impact metamorphism.

PETROLOGIC DESCRIPTIONS AND ANALYSES

Several ordinary chondrite meteorites were examined in this study, which already have basic descriptions in the Meteoritical Bulletin Database. Key textural observations are given below.

Hamilton (L6)

The 68 kg Hamilton meteorite was originally classified as an L6 ordinary chondrite. In the samples observed in this study only sparse remnants of radial pyroxene and barred olivine chondrules were observed (3 per thin section; Fig. 1A). The silicate minerals are strongly recrystallized, with coarse clear maskelynite grains after plagioclase being preserved, some of which significantly exceed 100 μm in size (Fig. 1B).

Examples of metal-sulfide textures found in Hamilton are shown in Figs. 1C–F. In every composite metal-sulfide grain there is a complex finely intergrown mixture of troilite and Fe-Ni metal. This texture has been described previously as “fizz texture” (Scott 1982), but the term mosaic texture is used here, as “fizz” implies involvement of a gaseous phase in its formation. Some of these composite grains contain single-phase domains, which can be either Fe-Ni metal or troilite, but not both. The bulk composition of mosaic-textured domains is dominated by FeS, although the metal/troilite ratio varies (from ~0.10 to 0.53; based on area analyses of reflected light photographs using Adobe Photoshop), being significantly higher in grains containing a metal-only domain. In these grains, the contacts between mixed metal-sulfide regions and metal-only domains are highly irregular, such that the metal appears to have been consumed by the metal-sulfide mix. The metal-only domains are typically dominated by kamacite (typically ~$Fe_{93}Ni_7$; Fig. 1), whereas the mosaic-textured domains are richer in taenite (typically ~$Fe_{65}Ni_{35}$; Fig. 1) and tetrataenite, and thus relatively Ni-enriched. Similarly, the periphery of many mosaic-textured domains are kamacite-rich, whereas the interiors are taenite- and tetrataenite-rich (Figs. 1C and D). Some metal-only domains preserve zoned taenite + kamacite textures (Figs. 1E and F) similar to those reported for slowly cooled, mildly shocked H and L chondrites (Reisner and Goldstein 2003). The zoned taenite in these grains is coarsely plessitic, whereas those described by Reisner and Goldstein (2003) have cloudy zone structure. In these cases, the taenite appears to have been preferentially incorporated into the mixed metal-sulfide domain relative to kamacite (Figs. 1E and F). Most composite grains have approximately equant morphologies and none exceed 2 mm in diameter, although the margins of some are characterized by short metal-sulfide veins propagating a short distance between adjacent silicate grains. Isolated metal-only, as well as troilite-only, grains also occur.

Several small (5–20 μm) irregular patches of silicate glass mixed with spherical inclusions of metal ± sulfide also occur in Hamilton (Fig. 2A). These are developed at the contacts between metal, or composite metal-sulfide grains, and silicate minerals. Where composite metal-sulfide grains are involved there is only minor incorporation of metal + sulfide into the silicate glass. In several glass patches, the spherical inclusions are Fe-Ni metal only, with no sulfide. There are also a small number of glass-filled veins with sharp, well-defined margins. These vary from being glass-dominated veins with sparse spherical inclusions of troilite ± metal, to narrow troilite-dominated veinlets with

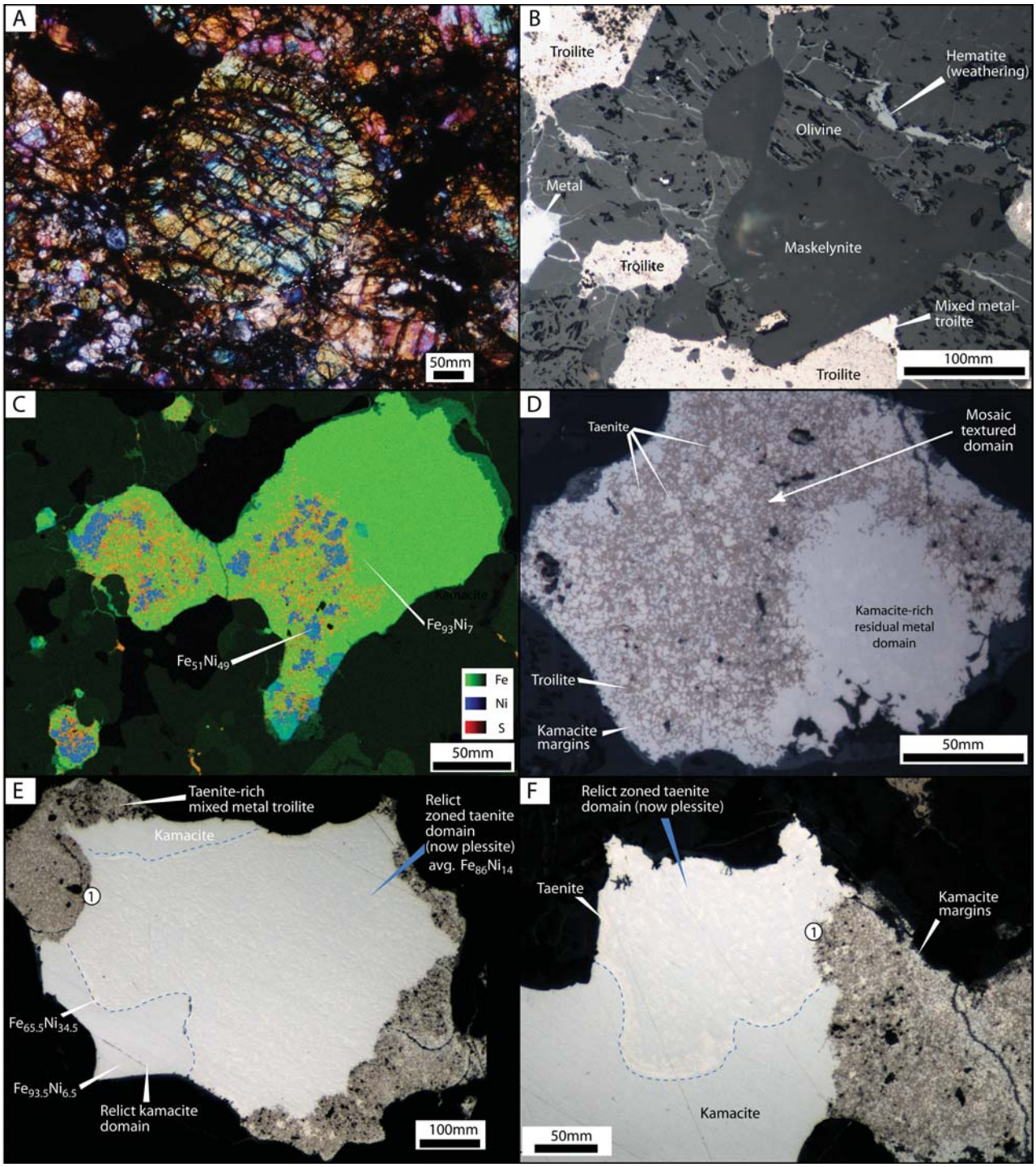

Fig. 1. Textures observed in the Hamilton meteorite. A) Relict barred olivine chondrule. Planar fractures are also visible in the olivine (crossed nichols). B) Coarse-grained (>100 μm) maskelynite after plagioclase (reflected light). C) Multielement X-ray map showing the distribution of kamacite (green), taenite/tetrataenite (blue) and troilite (orange) in a composite metal-troilite grain from Hamilton. Image generated on a JEOL 8500F-CL HyperProbe (field-emission gun electron probe microanalyzer) operating at 12 keV, pixel size of 0.5 μm. D) Composite metal-sulfide grain in Hamilton showing corroded residual metal domain and taenite-rich mixed metal-troilite domains (reflected light). The contrast has been enhanced to highlight differences in the distribution of kamacite (bluish white; most of the residual metal and periphery of mixed domain) and taenite (yellowish white; interior of mixed domain). E and F) Composite metal-sulfide grains in Hamilton showing preferential corrosion at (1) of residual zoned taenite domains (outlined in dashed blue), relative to kamacite, by mixed metal-troilite (reflected light; contrast enhanced as for D).

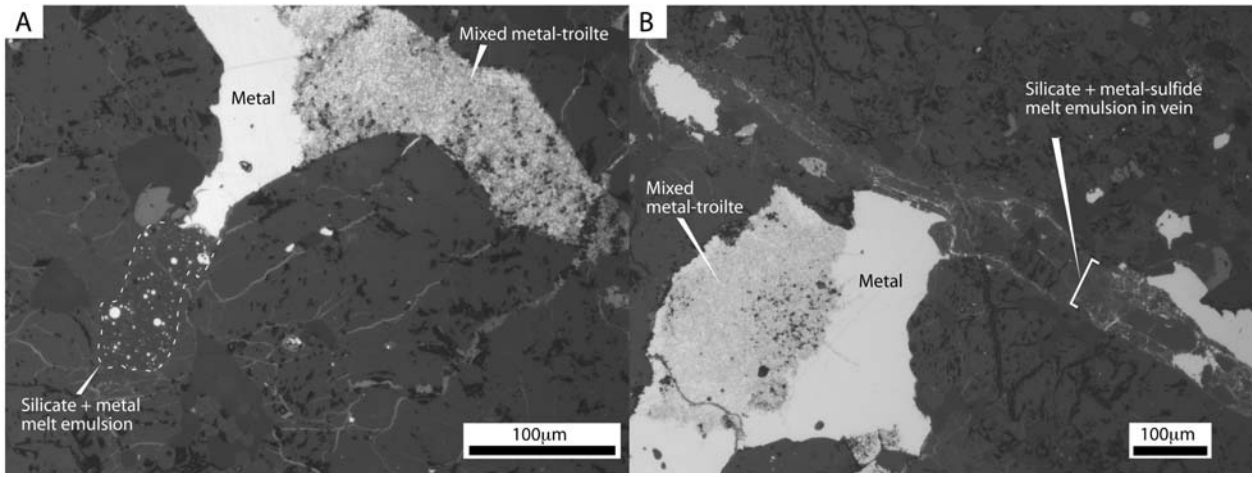

Fig. 2. Interpreted impact-melt textures preserved in Hamilton. A) A patch of slightly mobilized silicate glass containing spherules of Fe-Ni metal (no sulfide), developed at a contact between metal and plagioclase (reflected light). The mixed metal-troilite domain is not mobilized. B) A veinlet filled with silicate glass included by micro-spherules of sulfide ± metal. The vein cuts sharply across a composite metal-sulfide grain, with no draining of the mixed metal-troilite domain (reflected light).

spherical silicate glass inclusions within the wider vein (Fig. 2B). Overall vein widths vary from 1–500 μm. There are many examples where these veins cut abruptly across composite metal-troilite grains, such that the truncated portion appears to be incorporated into the vein, although the composite grains do not appear to be draining into the veins. Composite grains immediately adjacent to, but not intersected by, the glass-filled veins, are undisturbed.

Northwest Africa (NWA) 869 (brecciated L4–6 chondrite)

NWA 869 has been categorized as a brecciated L4–6 ordinary chondrite (Connolly et al. 2006), and the sample examined in this study consists of a single clast of L6 material. Solidified impact melt patches are recognized in this meteorite, which exist as small irregular pockets of either silicate glass with spherical metal and/or sulfide inclusions, or metal with spherical silicate glass inclusions (Fig. 3B, see also Fig. 2A). Petrologic analysis of NWA 869 found that these melt pockets are dominated by plagioclase-composition glass, Fe-Ni metal, troilite and chromite in order of abundance, whereas unmelted domains are dominated by olivine and pyroxene. The distribution of these melt domains suggests that melting to produce these isolated pockets was localized at contacts between metal, troilite or chromite and silicates. Even in conjoined metal-troilite grains, melting involved either (1) Fe-Ni metal and silicate only (Fig. 3B), (2) both metal, troilite and silicate, forming mixed silicate-metal-sulfide melts, or (3) troilite and silicate only. The boundaries between metal and troilite in composite grains are not more affected by melting than elsewhere (Fig. 3B). Melt patches are not interconnected at scales exceeding 2 mm. These melt emulsions (a melt emulsion consists of spherical inclusions of one melt phase inside another) have previously been recognized in other meteorites and represent immiscible mixing of metal and/or sulfide melt with silicate melt (e.g., Stöffler et al. 1991). Melt emulsion patches such as these are typically interpreted as having formed in response to shock resulting from a hypervelocity impact (e.g., Stöffler et al. 1991).

None of the conjoined metal-troilite grains in NWA 869 display the intimately mixed texture observed in Hamilton. Instead, most such grains consist of only one metal and one troilite domain, although some display the troilite-inclusions-in-metal texture described in Eldee 001 (below).

Chergach (brecciated H5)

Chergach is from a meteorite shower that occurred in Mali, Africa, in 2007, formally classified as a H5 ordinary chondrite. The sample examined in this study is highly brecciated, with thick, millimeter- to centimeter-scale glass-rich veins that cement minimally disturbed clasts (Fig. 3A). These clasts contain well-defined chondrules typical of petrologic type 5 (Fig. 3C). At micro-scale, textures characteristic of shock melting associated with hypervelocity impact are preserved in Chergach, recognized as regions containing variable proportions of silicate glass with spherical metal and troilite inclusions (cf. Stöffler et al. 1991). Unlike NWA 869, the melted domains occur as linked veins rather than sparse patches (Figs. 3A and 3D). These silicate melt veins are highly spatially focused zones that cut across all minerals, with minimal disturbance of material outside the vein. Generally, veins are volumetrically dominated by silicate glass, although narrower metal and/or sulfide veinlets are also observed within or at the vein margins (Fig. 3D).

Within the breccia clasts in Chergach, all composite metal-troilite grains show the same mosaic texture described from Hamilton. However, some of these mixed metal-troilite

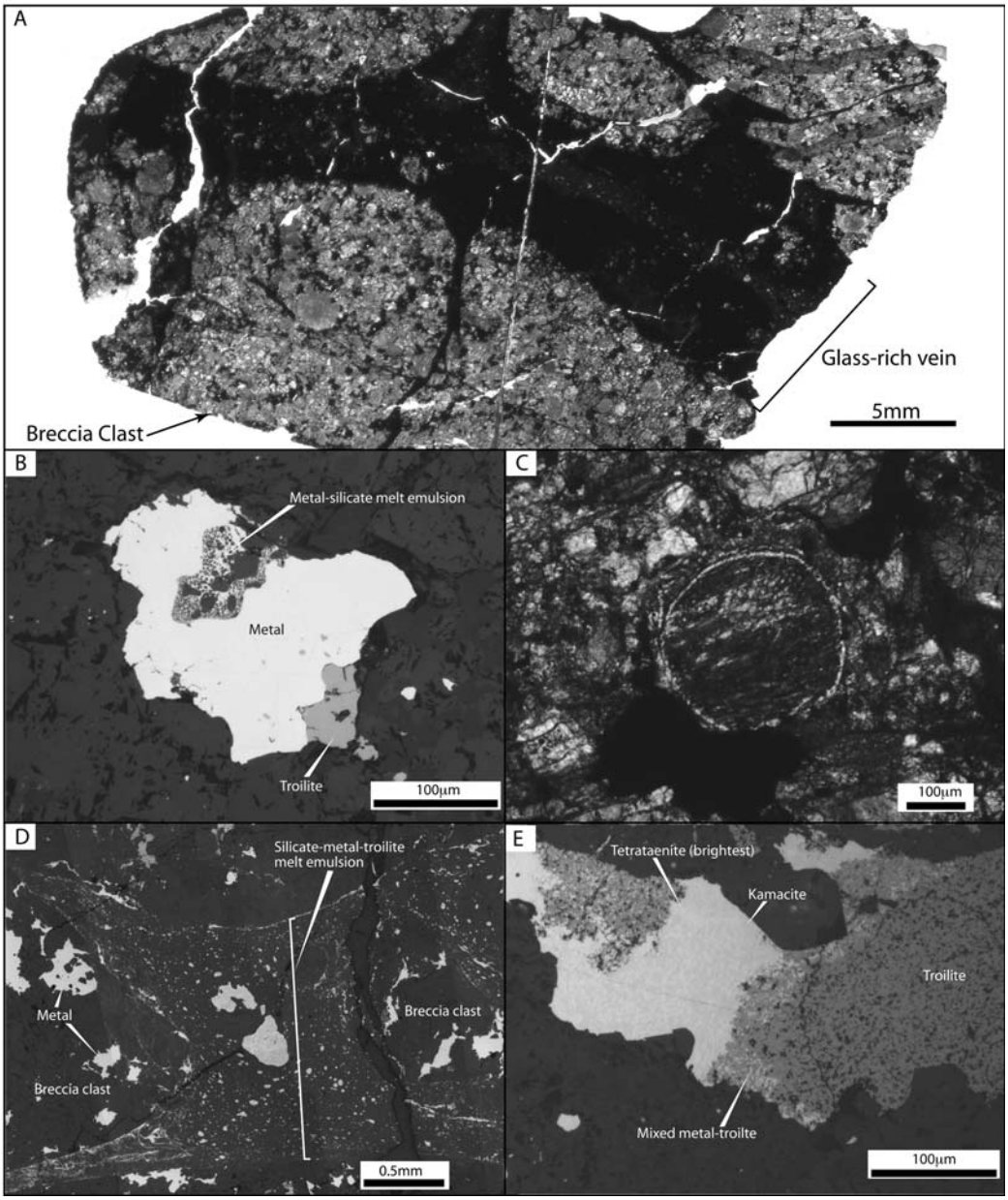

Fig. 3. Textures preserved in NWA 869 and Chergach. A) Plane polarized light scan of a thin section of Chergach, showing the distribution of glass-rich veins (black) and breccia clasts (rounded, textured, transparent areas). B) Spatially focused melting in NWA 869 developed at the contact between metal and silicate. There is no melting at the troilite-metal contact. The melt zone consists of silicate glass spheres in a matrix of metal, with a few small unmelted silicate clasts (reflected light). C) Moderately well-preserved olivine chondrule in Chergach, consistent with the H5 classification (greyscale image from crossed nichols). D) Vein textures associated with frictional melting along micro-shears in Chergach, showing immiscible colloids of silicate and metal + sulfide melt, which wrap around breccia clasts (reflected light). E) A composite metal-troilite grain inside a breccia clast in Chergach (reflected light, contrast enhanced). Mixed metal-troilite domains are dominated by troilite. The mixed metal-troilite domain separates residual troilite and metal. Exsolved tetrataenite (brightest) and kamacite (slightly less bright) are visible in the plessitic residual metal domain.

grains contain a metal-only domain and a troilite-only domain separated by the mixed material (Fig. 3E).

Eldee 001 (L6)

Eldee 001 is a typical L6 ordinary chondrite with a shock classification of S3, and no shock veins. Examples of the metal-sulfide textures found in Eldee 001 are shown in Fig. 4. Individual metal and sulfide grains are common in the sample, and there are also many conjoined grains. Many, but not all, of these conjoined grains consist of a large portion that is 100% troilite adjacent to a metallic portion that in some examples contains many small inclusions of troilite and trace inclusions of metallic copper. Plessite can be distinguished

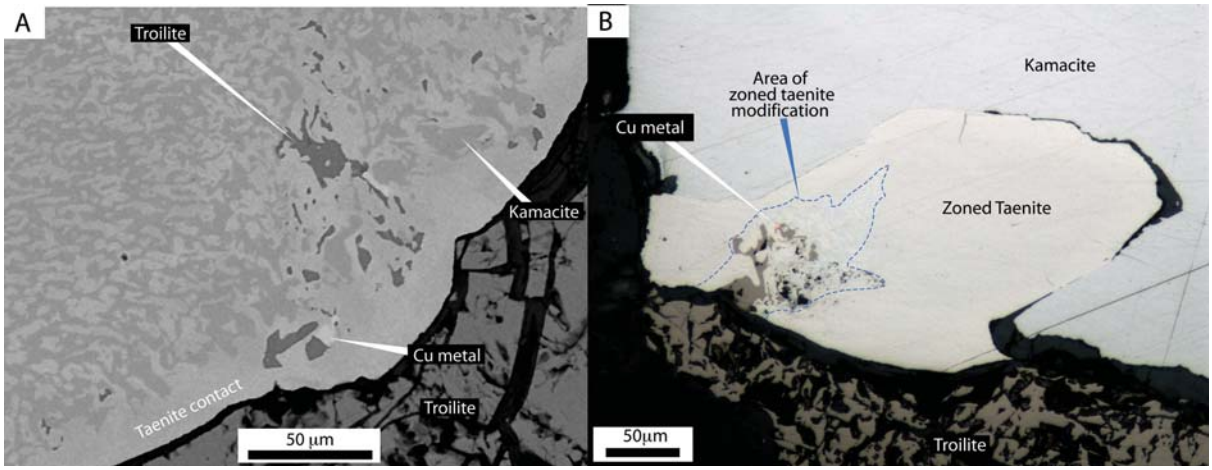

Fig. 4. Metamorphic metal-sulfide textures observed in Eldee 001. A) Back-scattered electron image of troilite and copper inclusions amongst plessitic metal, adjacent to a large troilite grain. Troilite and Cu metal inclusions are contained within Ni-rich taenite (close to tetrataenite in composition). The large troilite grain (bottom right) is rimmed by taenite. B) Zoned taenite + kamacite adjacent to troilite, with disruption to the zoned taenite by an area of troilite and Cu inclusions amongst plessite (reflected light; contrast enhanced).

within the metallic portion, and where troilite inclusions are present, these are dominantly surrounded by tetrataenite or Ni-rich taenite. Cu metal is typically associated with zones of troilite inclusions. The contacts between troilite and metal are typically taenite/tetrataenite-rich. Analyses indicate that the troilite inclusions and large troilite grains typically contain below detection Ni; Cu metal contains ~ 5–6 wt% Fe and 3.0 wt% Ni, taenite composition varies from 47.97–55.98 wt% Ni (the remainder being Fe); and kamacite contains on average 2.9 wt% Ni (analyses conducted on a Jeol 840A SEM operating at 20 kV).

This texture has been recognized in numerous other H, L, and LL chondrites classified from petrologic type 3 to 6 (Rubin 1994, 2004). Two hundred and ten meteorites of shock grade S1–2 were examined by Rubin (2004), of which 29.3% of the type 4 chondrites contained irregular FeS inclusions in metal, whereas 53.3% of type 5 and 52.7% of type 6 contained these inclusions (considerably less contained Cu metal inclusions). In a study focusing on metallic Cu Rubin (1994) found that at least 66% of ordinary chondrites contain this phase, dominantly at troilite-metal interfaces. Rubin (1994) also found that more highly shocked meteorites tend to contain more abundant Cu metal.

DISCUSSION

Distinguishing Between Syn-Impact and Post-Impact Melting

Impacts between asteroids release enormous amounts of energy, some of which is converted into heat. This heat is enough to cause melting of both silicates and the metal-sulfide assemblage in the vicinity of the impact, as observed in meteorites with melt breccias such as Chergach, although probably not enough to cause formation of large impact melt sheets (Keil et al. 1997). There are three different heating mechanisms responsible for producing this melt, two of which occur during crater formation and the other evolving after cessation of movement.

Heating associated with the impact-induced pressure wave is maximized at interfaces between high and low density phases (Stöffler et al. 1991). Because Fe-Ni metal and plagioclase are the highest and lowest density phases respectively, interfaces between these minerals are preferentially the focus of impact heating (Stöffler et al. 1991). In Figures 3B and 2A, textures of incipient impact melting directly associated with the passage of a pressure wave are displayed. In these samples (NWA 869 and Hamilton, respectively), metal grains were partially melted and mixed immiscibly with silicate melt, as were many sulfide grains. Because it is the contacts between the metal and silicate that are the focus of heating, both metal and silicate melt are produced, and the resulting texture is almost invariably that of immiscible mixing of the two melts, producing an emulsion. Although composite metal-sulfide melts are also produced by this process, the samples examined here show that the contacts between troilite and metal were not affected more than isolated metal grains (Fig. 3B). Yet, the minimum melting temperature of Fe,Ni + FeS in chondrites is <988 °C, whereas Fe metal melts at 1538 °C. Furthermore, the examples of composite metal-sulfide melts that do exist range significantly in bulk composition from sulfide-rich to metal-rich, rather than being consistently of cotectic composition. These observations therefore indicate that initial impact heating is extremely spatially focused (Stöffler et al. 1991).

Heating instead associated with extremely high-strain deformation along spatially focused micro- to mesoscale shear planes also produces composite metal and/or sulfide melts immiscibly mixed with silicate melt (Van der Bogert

et al. 2003). This shear heating is associated with crater excavation and rebound, and thus only lasts for seconds to minutes, depending on the size of the impact and the rheology of the target material (cf. Melosh and Ivanov 1999). Composite silicate-metal-sulfide melt emulsions are again produced because the shear planes cut indiscriminately across the rock causing frictional heating of all phases. However, localized micro-scale structural dilatancies produced by this shear deformation promote segregation of small aliquots of metal and/or sulfide melt from silicate melt to produce narrow veins of the former (cf. Rushmer et al. 2005). The textures produced in this case are also distinct from those produced by static heating in that the metal ± sulfide accumulations produced during impact tend to be found in micro- to mesoscale veins that range in composition from 100% metal, through mixed compositions, to 100% sulfide.

The third mechanism that may be capable of causing impact-related melting is not so much a heating event, but rather a dissipation of thermal energy after the impact event that promotes localized cooling and heating within a given volume of impacted rock. Both of the impact-generated heating mechanisms described above produce a heterogeneous heat distribution focused at grain boundaries and along shear planes, with localized temperatures demonstrably exceeding the melting point of Fe-Ni metal (>~1500 °C). Large volumes of melt breccia can occur as thick sheets that blanket the bottom of impact craters, or as extensive pseudotachylite dykes beneath a crater, and some meteorites have been interpreted as having been sourced from magmatic dykes beneath impact craters (e.g., Folco et al. 2004). After these short-lived heating events have ceased, heat diffuses from the localized high-heat domains into adjacent unheated domains, driving towards thermal equilibrium, a process analogous to contact metamorphism around magmatic intrusions on Earth. This process is thus referred to here as post-impact metamorphism, to distinguish it from radiogenic metamorphism.

If enough thermal energy is generated by the two short-lived impact heating mechanisms, thermal re-equilibration may subsequently allow significant volumes of rock to exceed the melting point of the metal-sulfide assemblage, or even the silicate assemblage, for a short time. Metal-troilite melts produced through this static heating would form in situ, as localized pockets of melt dominated by FeS, dispersed throughout the appropriately heated region. Because this post-impact metamorphism takes place in a static strain environment, after the impact event, there is no mechanism to drive melt mobilization, although the positive volume change associated with melt formation may cause cracking and minor mobilization (cf. McCoy et al. 1997). Consequently, there is no reason why these static metal-sulfide melts would incorporate immiscible silicate melt. The result is that during hot post-impact metamorphism, every composite metal-troilite grain in a given sample melts and then cools rapidly in situ, each producing a finely mixed metal-troilite texture with FeS-rich bulk composition, which is distinctly different to textures produced through syn-impact melting.

Development of Metal-Troilite Mosaic Textures

In discussing the origin of rapidly solidified metal-troilite grains in meteorites, Scott (1982) recognized a non-dendritic metal-troilite texture present in some chondrites; the same texture as represented in Figs. 1C–F and 3E. It was suggested that this mosaic texture may have crystallized during low temperature annealing of a metal-sulfide glass, which itself formed through quenching of syn-impact melt. This interpretation was based on the concept that troilite can melt when subjected to heavy shock (≥75 GPa), incorporate adjacent metal and then quench to glass. However, more recent work has found this mosaic texture in ordinary chondrites with shock grades of only S1 and S2 (Rubin 2004), indicating that high shock pressure is not responsible. This conclusion is supported by the observation that mosaic texture is inconsistently developed in even the most shocked meteorites (Bennett and McSween 1996). Furthermore, metallurgists have found that only a small number of metal-semimetal liquids can be quenched to glasses in the laboratory (typically requiring quench rates of $\geq 10^6$ Ks^{-1}) and iron-nickel-sulfide liquids are not amongst these (e.g., Polk and Giessen 1978); even with cooling rates of 10^{12} Ks^{-1} crystallization cannot be prevented for a large number of these liquids (Sommer 1985). Complex experimental procedures are needed to achieve these extreme quench rates, which are not possible in metal-troilite grains insulated amongst low thermal conductivity silicate grains within asteroidal regoliths and crusts. Thus, some other mechanism is required to form the mosaic texture.

During the comparatively slow radiogenic metamorphism of the chondrite parent bodies, which lasted <5 Ma (Trieloff et al. 2003), the metal particles diffusively re-equilibrated to homogenous taenite corresponding to their respective bulk compositions in areas where temperatures exceeded the taenite solvus (i.e., in petrologic types 4–6; Reisner and Goldstein 2003). Then, during slow cooling, two types of metal textures evolved; polycrystalline taenite grains transformed into zoned taenite + kamacite, and monocrystalline particles became zoneless plessite (Fig. 5A; see Reisner and Goldstein 2003). Figure 6 is a phase diagram in the system Fe-Ni-S, which shows how the preservation of zoned taenite + kamacite, or lack thereof, affects the initial melting temperature of the metal-sulfide assemblage during heating. On this diagram, the bulk compositions of metal particles for H, L, and LL chondrites are plotted. If the temperature of radiogenic metamorphism was hot enough, the homogenized taenite particles in ordinary chondrites would have started to melt, provided that they were in contact with troilite, as temperatures approached 988 °C (temperatures

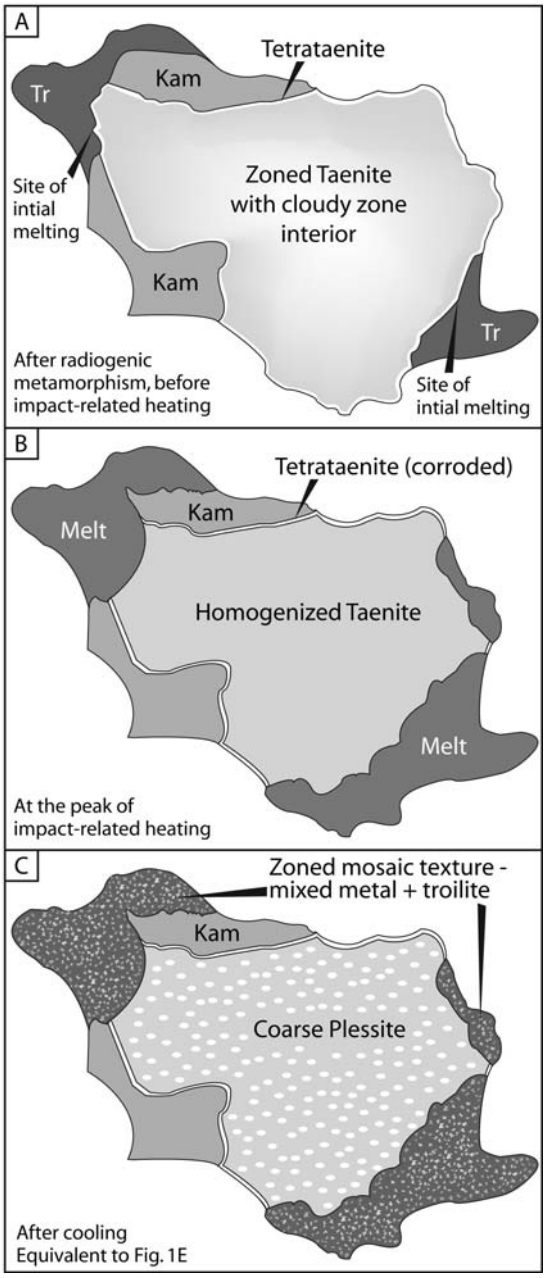

Fig. 5. Illustration of the progressive melting of a conjoined metal-troilite particle during post-impact metamorphism (the sketch replicates Fig. 1E). A) After radiogenic metamorphism, zoned taenite + kamacite grains evolve during cooling (Reisener and Goldstein 2003), some of which may be adjacent to troilite particles. The zoned taenite has a sub-micron cloudy zone textured interior. B) Then, approaching the peak temperature of post-impact metamorphism via rapid heating, taenite and tetrataenite are consumed by melting in preference to kamacite. Diffusion causes the previous sub-micron cloudy zone texture to homogenize, and partial corrosion of the tetrataenite rim originally separating kamacite from zoned taenite. C) During subsequent rapid cooling the melt domains fractionate on a microscopic scale, producing kamacite-rich margins and taenite-rich cores. Fast cooling transforms homogenized taenite to martensite and then plessite texture in the relict zoned taenite domains within the residual metal.

closer to 900 °C are needed for LL chondrites; Fig. 6). The melt produced through this slow heating would have a composition close to 85 wt% FeS and 15 wt% Fe-Ni(-Cu). The silicate assemblage would not have melted until temperatures beyond ~1100 °C were reached (Jurewicz et al. 1995).

The chondrite parent bodies were affected by large impacts during (Hutchison et al. 2001) and after (e.g., Bogard et al. 1995) this cycle of early radiogenic metamorphism. If post-impact metamorphism affected type 4–6 chondrites during the peak of radiogenic metamorphism (impacts would need to be large enough to reach appropriate depths), the resulting metal-troilite melting relationships would be no different to those indicated above because the phases involved are homogenized taenite and troilite. In cases where instead post-impact metamorphism occurred well after radiogenic metamorphism, the melting relationships would have been significantly different. In post-impact metamorphism, heating is extremely rapid, so the zoned taenite + kamacite particles that developed after radiogenic metamorphism would not have had time to diffusively re-equilibrate to homogenous taenite. In this case, unequilibrated metal grains, containing taenite (γFe), tetrataenite, and kamacite (αFe) (typical meteoritic exsolved metal compositions are shown on Fig. 6) are subject to melting over a broader range of temperatures, where they are in contact with troilite. In Fig. 6, two different phase fields are contoured for temperature; a grey shaded Liquid field (L), and a dash-outlined, triangular shaped γFe + FeS + Liquid field. Both fields migrate toward more Fe-rich compositions with increasing temperature (see Villars et al. 1995 for more detail).

Importantly, the information in Fig. 6 indicates that Ni-rich taenite and tetrataenite in contact with troilite can start to melt as temperatures approach 850 °C and progress through 860 °C, which is approximately 130 °C lower than the initial melting temperature of radiogenic metamorphism (for H chondrites). Progressively less Ni-rich taenite melts as temperatures approach and then exceed 900 °C (illustrated in Fig. 5B), and kamacite starts to melt as temperatures approach 988 °C. However, equilibrium within the melt is achieved very quickly (low melt viscosity allows rapid element diffusion), and equilibration between Ni-rich melt and kamacite will cause some melting of the latter as temperature increases beyond initial melting. The melt compositions also vary considerably as melting progresses. At 850 °C, the melt composition (which plots where the γFe + FeS + Liquid field joins the Liquid field; the cotectic) is Ni-rich (~45% Ni) and sulfide-poor (~68% Fe-Ni-sulfide) compared to the melt composition that would develop through radiogenic metamorphism.

Diffusion of Ni into melt from residual metal is approximately nine orders of magnitude faster than in silicate diffusion (cf. Hopfe and Goldstein 2001; Petry et al. 2004;

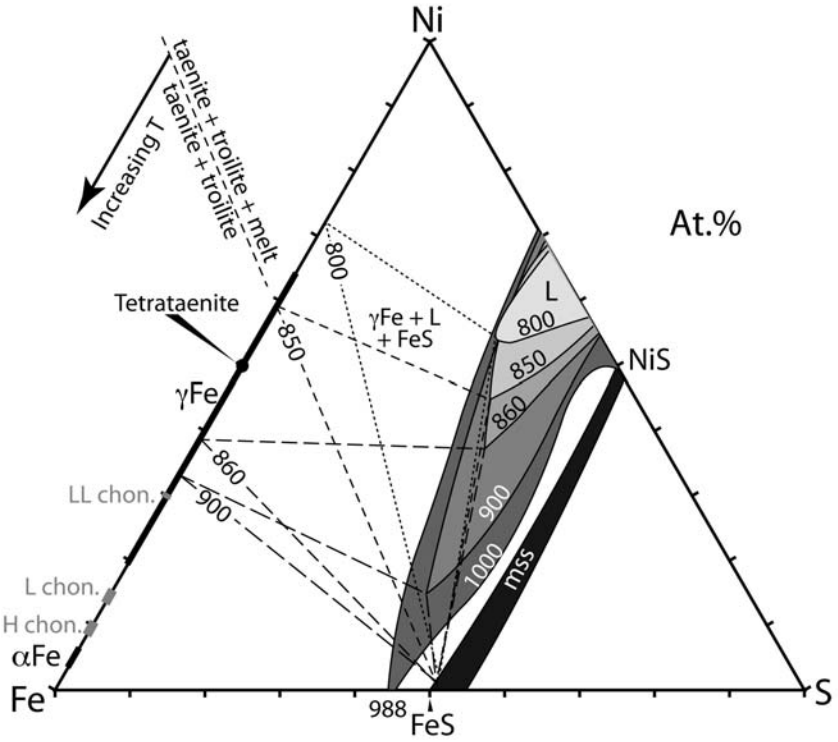

Fig. 6. Fe-Ni-S ternary phase diagram (At%). The typical bulk compositions of metal grains in H, L and LL chondrites are plotted in grey on the Fe-Ni join. The compositions of kamacite (αFe) and taenite (γFe) found in meteorites are also plotted on the Fe-Ni join in thick black lines. The grey shaded fields represent the expansion of the liquid field (L) with increasing temperature (°C). Mss is monosulfide solid solution, of which troilite (FeS) is an end-member. The dashed triangles represent the changing position of the γFe + FeS + Liquid field with increasing temperature. 988 °C is the eutectic in the pure Fe-FeS system; the cotectic in the Fe-Ni-mss system links this with the joins between the liquid field and the γFe + FeS + Liquid field. Compiled from a series of isothermal phase diagrams in Villars et al. (1995).

Saikumar and Goldstein 1988). This rapid Ni partitioning, together with the early melting of Ni-rich taenite, has two implications for understanding textural development. Firstly, given time, Ni will diffuse into the melt from any unmelted metal grains in contact, thereby making the residual grains more Fe-rich. Secondly, as the melt cools, more Fe-rich metal will crystallize first, typically at the margins of the melt. During rapid cooling, the metal-sulfide melt will unmix as it crystallizes to form a finely intergrown texture of troilite and metal, with a composition dominated by troilite and varying as a function of Ni content (as per Fig. 6). Therefore, the resulting texture should consist of residual kamacite-rich metal grains in contact with a mixed metal-sulfide domain that itself has relatively kamacite-rich margins and taenite-rich cores. If a melt is instead instantaneously quenched there is no time for micro-scale fractionation and no zoning can develop within the melt domain. Similarly, if the duration of time that a melt domain remains in contact with residual metal is minimized, then little diffusion of Ni into the melt can take place, and some preservation of the zoned taenite + kamacite particles should be expected. However, because elemental diffusion is much faster in metallic liquids than solids, the zoned melt domains will develop rapidly (in seconds to minutes, based on the unmixing of metallic melts during quenching observed by experimentalists), whereas Ni-depleted zones adjacent to melt in residual metal will develop comparatively slowly (it would take ~1 year for a heterogeneous 10 μm taenite-kamacite grain to fully homogenize at 900 °C; cf. Hopfe and Goldstein 2001; Reisener and Goldstein 2003). Therefore, if the heating-cooling cycle takes place in the space of seconds to weeks, the melt domains would become zoned, whereas the residual metal would partially retain the relict zoned taenite-kamacite texture (Fig. 5C). In addition, rapid cooling should cause transformation of the relict zoned taenite domains to martensite and then plessite (cf. Hutchison and Bevan 1983; Reisner and Goldstein 2003; Rubin 1990). A further important point is that if Ni diffusion in metal is minimal then there can be almost no elemental diffusion amongst silicate minerals.

The motivation behind Scott's (1982) suggestion that the mosaic texture formed through extreme quenching of melt to a metal-sulfide glass, followed by solid-state exsolution, was that it appears different to the dendritic texture typically found in quenched impact emulsions. However, instead of quenching to glasses, metal-sulfide melts unmix during rapid cooling to form a finely intergrown fabric of metal and sulfide phases that varies in texture as a function of the quench rate, the proportion of phases and the interfacial energy between

the phases (e.g., compare quenched melt textures in Mavrogenes et al. 2001; Sparks and Mavrogenes 2005; Tomkins and Mavrogenes 2002; Tomkins et al. 2007). It is suggested here that the mosaic texture differs from the dendritic texture because during the cooling stage of post-impact metamorphism, all of the factors listed above are different to the situation in impact melt emulsion quenching. In the post-impact metamorphism situation, the cooling rate is likely to be slower, the metal/sulfide and Ni/Fe ratios in the melt are higher, and the temperature is likely to be lower, when compared with the impact melt emulsion situation. These factors, particularly the compositional differences, will cause divergence in the interfacial energies between crystallizing phases, leading to the observed textural differences.

Distinguishing Post-Impact from Radiogenic Metamorphism in Hamilton and Chergach

Metal-sulfide textures within Hamilton (Figs. 1C–F) are consistent with partial melting in that all grains where metal and sulfide co-exist are dominated by finely inter-grown mixtures of both components (the characteristic texture of quickly cooled metallic melts). However, issues remain regarding the timing of this partial melting.

The shock grade of Hamilton is estimated at S5, based on the observation of ubiquitous maskelynite and planar deformation features in olivine (cf. Stöffler et al. 1991). The low viscosity of metal-sulfide melts means that they are easily mobilized by deformation associated with impacts (cf. Rushmer et al. 2005). Therefore, the observation that there is minimal bleeding of melt from the composite metal-troilite grains where they are cut by the glass-filled micro-shears (Fig. 2B) implies that they were solid at the time of impact (i.e., only the sheared portion melted during the impact). In Fig. 2A a localized, slightly mobilized patch of immiscible Fe-Ni metal melt in silicate melt (requiring a localized temperature exceeding 1535 °C, the melting point of Fe) can be seen adjacent to a domain of mixed metal-troilite material that is unmobilized. This texture again suggests that the metal-troilite domain was immobile and thus solid at the time of impact. The observation (Figs. 1C–F) that the mixed metal and troilite are in near-cotectic proportions (FeS-rich) throughout Hamilton suggests that melting took place under near-equilibrium conditions. Although there are silicate inclusions in some metal-sulfide grains, these tend to be rare coarse grains rather than numerous tiny spheroidal particles, suggesting that they were not immiscible melts and therefore not of impact origin. Furthermore, the ubiquitous distribution of the metal-troilite melt textures indicates that the entire sample exceeded this temperature, which is different to the highly spatially focused heating generated during impacts. Thus, the metal-sulfide melts shown in Fig. 1 did not form during the impact event responsible for the melt emulsions shown in Fig. 2 (i.e., they formed either before or after). Hamilton contains only chondrule relicts and large maskelynite (after plagioclase) grains, indicating that it reached high temperatures through radiogenic metamorphism. These observations therefore raise the question of whether the metal-sulfide melt textures in Hamilton reflect radiogenic rather than post-impact metamorphism.

Because the CaO content of orthopyroxenes in this meteorite is dominantly below 1.00% (range: 0.68–1.24 wt%), the temperature of radiogenic metamorphism is unlikely to have been high enough to cause melting of the metal-troilite assemblage (cf. Mittlefehldt and Lindstrom 2001). The comparatively long duration of radiogenic metamorphism would have allowed enough time to diffusively equilibrate the CaO content in orthopyroxene to >1.0% throughout the sample at the temperatures required for metal-troilite melting (cf. Lindsley 1983). Furthermore, the duration of the alternative post-impact metamorphism must have been short enough for heat to dissipate before the pyroxene chemistry was reset. This conclusion is supported by the metal-troilite textures. In particular, the relict zoned taenite + kamacite textures in residual metal shown in Figs. 1E and 1F are thought to form during cooling after radiogenic metamorphism (Reisner and Goldstein 2003), so their existence is evidence that the mosaic texture formed during a secondary heating process. The observed Ni zoning in the mosaic-textured domains suggests that this was not an instantaneous melting and quenching process; time was needed for diffusion to occur. However, the textures preserved in residual metal suggest that there was only minor solid-state diffusion of Ni during melting. Furthermore, the plessite texture replacing what was zoned taenite is likely to have formed after the original cloudy zone texture homogenized at peak temperature, then transformed to martensite, and then plessite during rapid cooling (compare Figs. 1E and 1F here with Figs. 2–4 in Reisner and Goldstein 2003). These observations therefore confirm that the heating and cooling cycle responsible for the mosaic texture in Hamilton was short-lived. There are no signs of metamorphic melting of the silicate assemblage, indicating that the peak temperature did not exceed 1100 °C.

Radiogenic metamorphism in Hamilton is thus interpreted to have reached conditions of between 750–950 °C (based on the preservation of chondrule relicts, size of maskelynite grains, and pyroxene composition), consistent with petrologic type 6. The observed metal-troilite melting, and lack of silicate melting, constrains the peak temperature of post-impact metamorphism to between 850 °C and 1100 °C. Furthermore, since kamacite appears to have participated in the melting process (Figs. 1C–F), it is likely that the peak temperature significantly exceeded 900 °C (Fig. 6). During this secondary metamorphic event, each composite metal-troilite particle in Hamilton melted and then underwent minor

localized micro-scale fractionation as the melt crystallized, as suggested by the kamacite-enriched margins and taenite-rich cores of the melt domains (Figs. 1C and 1D). This fractionation also promoted development of heterogeneity in the metal/sulfide ratio, which could otherwise have been used to better constrain the peak temperature from phase relations. The heating-cooling cycle responsible for the textures in Hamilton is interpreted to have been short, lasting <1 year, based on the partial preservation of zoned taenite + kamacite in residual metal (Figs. 1 E and 1F).

This post-impact metamorphism melting can be seen to have also happened in Chergach, in which a pseudotachylite melt network can also be observed (Fig. 3A). All composite metal-troilite grains in the small breccia clasts of Chergach show textural evidence of cotectic melting (Fig. 3E), developed under thermal near-equilibrium (based on their consistently FeS-rich, near-cotectic compositions). These cotectic melts are free of immiscible silicate melt spherules and show minimal melt mobilization, implying that the temperature homogeneously exceeded ~850 °C throughout the sample in a quiescent environment. In contrast, the pseudotachylite melt emulsion network in Chergach (Fig. 3D) contains abundant evidence of disequilibrium metal ± troilite melt migration in a deforming environment (involving metal ± troilite melt globules with far from cotectic compositions). In such a violently disrupted meteorite, the composite metal-troilite grains preserved in the breccia clasts must have been solid during shearing and breccia development for them to have remained largely unmobilized, implying that they melted in response to thermal re-equilibration after deformation had ceased. Whether the source of the heating for post-impact metamorphism was the Chergach pseudotachylite or a nearby sheet of melt or melt breccia cannot be determined from the sample examined here, although the volume of pseudotachylite would need to be large to generate enough heat. In Chergach, it is simple to determine that the cotectic metal-troilite melting developed in response to post-impact heating rather than radiogenic metamorphism, because the well-preserved chondrules indicate that the maximum temperature of the latter could only have reached conditions consistent with petrologic type 5.

Rare composite grains in Chergach that consist of a metal-only domain, a mosaic textured domain and a sufide-only domain (Fig. 3E), indicate that the peak temperature did not prevail for long enough to achieve complete thermochemical equilibrium (at equilibrium there should be melt + one solid phase only). The sample of Hamilton examined in this study does not contain these slightly-out-of-equilibrium textures, suggesting that supersolidus temperatures prevailed for longer in this meteorite. The low proportion of impact melting focused at grain boundaries and along shear planes in Hamilton compared to Chergach implies that less thermal energy was imparted to the former during impact, and thus it might be expected that post-impact melting should be less likely or perhaps milder in the former. However, such an interpretation depends on how much impact-affected material surrounded and insulated the respective meteorite samples. For example, a breccia clast of chondritic material from near the center of a large impact structure, surrounded by numerous zones of spatially focused impact melt development, would have experienced a more prolonged period at high temperature than a similar clast within a distal pseudotachylite dyke.

Origin of Troilite (± Cu Metal) Particles in Plessite (Eldee 001)

During heating of metal-sulfide assemblages, textures can develop that resemble those produced by partial melting. These textures can, however, be explained as a product of subsolidus chemical transfer. Figure 4 shows examples of co-existing FeS, Fe-Ni metal, and Cu metal in the L6 chondrite Eldee 001, textures that have been noted in many other chondrites (Rubin 1994, 2004). In this figure, finely intergrown mixtures of troilite and plessitic metal can be seen within the metal-dominated part, resembling the texture produced by quench crystallization of metal-sulfide melts. Observations and analyses show that troilite within the metal is associated with Ni-rich taenite and tetrataenite rather than kamacite, that small inclusions of native Cu are also present in these zones, and that there is <25% troilite in the metal. Observation of these textures in some petrologic type 3 and 4 and many petrologic type 5 and 6 ordinary chondrites has been used previously to argue for shock melting, followed by annealing, of the metal-sulfide assemblage (Rubin 1994, 2004). Others have suggested that these complex kamacite-taenite-troilite-native Cu associations develop through low temperature exsolution from a high temperature sulfide solid solution phase contained within the metal, and are unrelated to shock processes (Chennaoui Aoudjehane et al. 2007; El Goresy 2006). A variation on this second explanation, mainly relating to how the metal becomes sulfur-enriched prior to cooling, is offered here.

During heating of the assemblage Fe + FeS, sulfur must be liberated as temperature increases. Figure 7 shows the path taken during metamorphism, in fS_2-temperature space, of this assemblage in meteorites, based on the well-established Fe-S phase diagram of Toulmin and Barton (1964). At low temperatures (point 1) the iron sulfide phase may initially be pyrrhotite ($Fe_{1-x}S$) rather than troilite (Lauretta et al. 1997), particularly in carbonaceous chondrites. As the assemblage heats up, the path on Fig. 7 moves to the right and small amounts of sulfur are gradually driven from the pyrrhotite, until at point 2 it becomes stoichiometric FeS, which is the mineral troilite:

$$\underset{\text{pyrrhotite}}{Fe_{1-x}S} + \text{heat} = \underset{\text{troilite}}{FeS} + \underset{\text{sulfur}}{xS_{2(g)}} \quad (1)$$

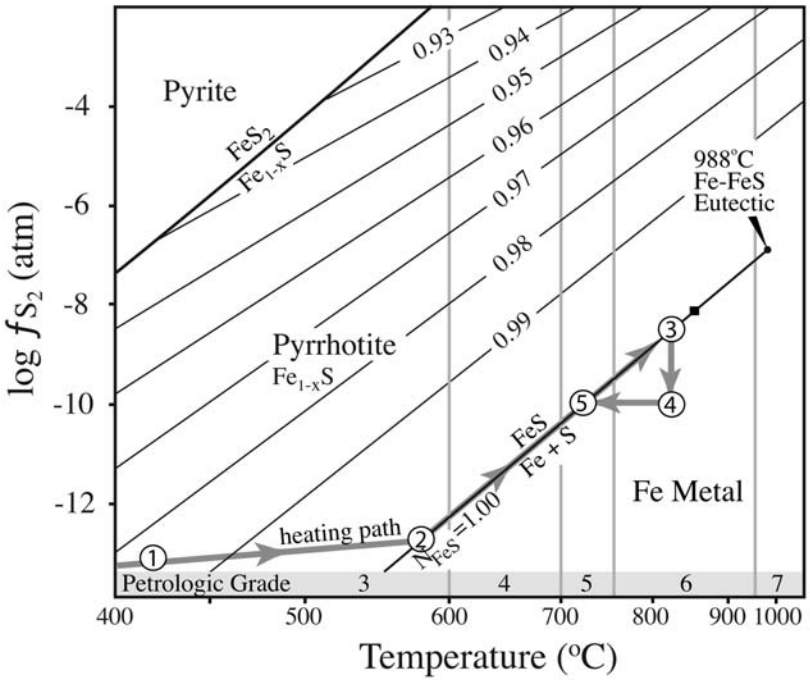

Fig. 7. Log fS_2 versus temperature diagram showing the thermochemical path taken by conjoined metal-sulfide grains during subsolidus heating and cooling. The small black square near (3) is the approximate melting temperature of tetrataenite + FeS. Modified from Toulmin and Barton (1964).

At this point FeS is in thermochemical equilibrium with the metallic phase. From point 2 the heating path must track along the Fe-FeS curve to maintain thermodynamic equilibrium and in doing so sulfur is continuously released in small quantities:

$$\underset{\text{troilite}}{2FeS} + \text{heat} = \underset{\text{iron}}{2Fe} + \underset{\text{sulfur}}{S_{2(g)}} \quad (2)$$

The log fS_2 scale of Fig. 7 indicates that at low temperatures little sulfur needs to be liberated to maintain equilibrium, but at higher temperatures exponentially more sulfur is required. If the sulfur is somehow removed from the troilite-metal contact, the reaction will continue to produce more sulfur to maintain equilibrium. Lauretta et al. (1997) showed that sulfur diffuses away from devolatilizing sulfide crystals along concentration gradients, providing a mechanism to drive ongoing desulfurization of the troilite. At high temperatures (though still subsolidus), trace amounts of sulfur can dissolve in Fe that coexists with FeS. The solubility of sulfur in Fe metal is strongly dependant on temperature; at 800 °C, 0.010 at% S can dissolve, whereas at 911 °C, the maximum of 0.033 at% S is reached (above 911 °C Fe goes through a phase transition and sulfur becomes less soluble again; Kubaschewski 1982). Thus, if the peak temperature reached is considerably beyond 800 °C (but still below the melting temperature), for example at point 3 (Fig. 7), there may be many times more sulfur dissolved in Fe metal than can exist at lower temperatures. However, there is too much troilite in the Fe-Ni metal from the studied samples (ranging from <1% to ~25% FeS) for all of the sulfur to have been in solid solution in the Fe-Ni metal (cf. Kullerud and Yund 1962; Kubaschewski 1982; Villars et al. 1995). An alternative possibility is that if sulfur migrated into metal along concentration gradients (e.g., to point 4 on Fig. 7), it would react with the metal during cooling to produce new troilite (at point 5 on Fig. 7), by reactions such as:

$$\text{Kamacite} + \text{Sulfur} = \text{Troilite} + \text{Taenite} \quad (3)$$

or

$$\text{Taenite} + \text{Sulfur} = \text{Troilite} + \text{Tetrataenite}. \quad (4)$$

So as an example, taking a 1 µg volume of taenite (with 30 wt% Ni) within a much larger metal grain, 0.08 µg of sulfur needs to be added to make 0.28 µg of troilite + 0.79 µg of tetrataenite (using Reaction 4). The assemblage on the product side of this reaction matches the assemblage observed in Figs. 4A and B (the remaining taenite would be converted to martensite and then plessite during rapid cooling; cf. Reisner and Goldstein 2003)). Copper tends to stay with the Ni-rich domains because taenite can accommodate about 16 times more Cu than kamacite (Hansen 1958). As the reaction progresses, the residual Cu concentration increases until it reaches saturation and exsolves, explaining why Cu metal occurs at troilite-metal contacts (Fig. 4; cf. Rubin 1994). The observation that this texture dominantly occurs in conjoined metal-sulfide grains, and that the newly formed troilite occurs within the metal rather than rimming it, also implies that the liberated sulfur (from Reaction 2) migrates into the metal prior to the onset of Reaction 3 or 4. This sulfur migration

should drive production of more sulfur via Reaction 2 than would otherwise be possible. For these reasons the retrograde interpretation is preferred, although it is conceivable that Reaction 3 could also occur on the prograde path if externally derived sulfur is somehow introduced (raising the sulfur fugacity above the Fe-FeS curve of Fig. 7), in which case a texture of troilite rimming metal would be more likely (cf. Lauretta et al. 1997). The taenite-rich metal-troilite contacts (Fig. 4) imply that some retrogression also occurred at the main contact, indicating that not all of the sulfur migrated into the metal, or that nucleation of new troilite was most efficient where troilite already existed. Any similar setting where metal is being consumed is likely to cause exsolution of Cu metal.

Importantly, the resulting texture consists of small amounts of troilite contained within metal (typically <25%), rather than vice versa, and thus the bulk composition of the mixed metal-troilite domain is a long way from the Fe-FeS eutectic composition (85% FeS, 15% Fe), or Fe-Ni-FeS cotectic compositions (as little as ~68% sulfide). These composite grains therefore cannot represent annealed melts, because the large amount of adjacent troilite that is not mixed with metal would generate troilite-saturated melt compositions containing >~68% sulfide.

An explanation for why only 53% of type 5 and 6 chondrites of shock stages 1 and 2 contain these irregular troilite inclusions in metal is necessary. Because more shocked chondrites contain a higher abundance of Cu metal (Rubin 1994), it may be that rapid shock-related processes somehow play a role in formation of this texture. The observation that some shocked petrologic type 3 meteorites contain these textures (Rubin 1994) implies that heating via radiogenic metamorphism is not critical. Although the conditions required for petrologic type 6 should cause liberation of sulfur within troilite-metal pairs, the observation that only 53% of these contain irregular troilite inclusions in metal indicates that the texture is a consequence of a process that did not affect all meteorites to the same extent. Shock-related processes may consequently offer the best explanation. Moderate post-impact metamorphism can lead to short-duration heating events that consequently have minimal effect on silicate textures. It may be that shock wave propagation promotes development of defects in the metal structure (Fig. 8A), allowing enhanced diffusion of sulfur from adjacent devolatilizing sulfide during subsequent heating (Fig. 8B), and ultimately, progression of the reactions described during retrograde cooling (Fig. 8C). Prograde radiogenic metamorphism should also produce sulfur, but this sulfur may instead stay at grain boundaries (if defects in the metal structure have not been produced by impacts), ultimately producing a small amount of troilite during retrograde cooling that is indistinct from pre-metamorphic troilite. Further support for the suggestion that this texture is impact-related is given by the observation that within any

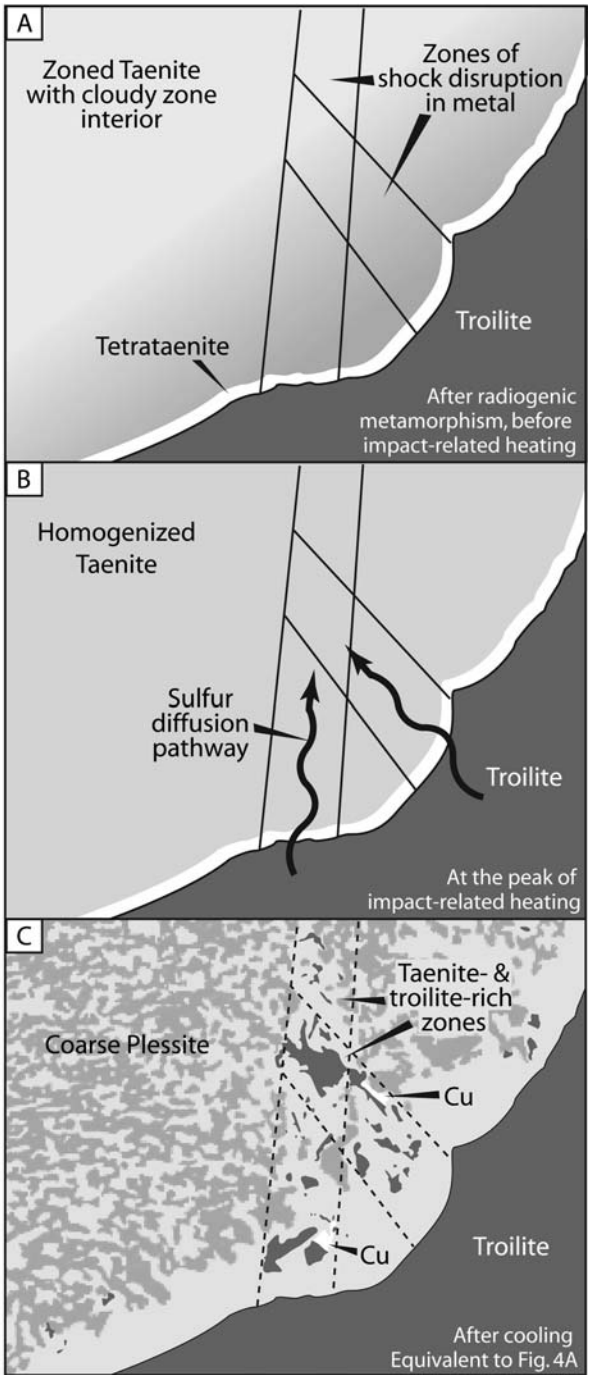

Fig. 8. Illustration of progressive metamorphism of a conjoined metal-troilite particle during post-impact metamorphism at sub-solidus conditions (the sketch replicates Fig. 4A). A) During impact, structural defects are imposed on a zoned taenite grain that evolved after radiogenic metamorphism. B) Then, approaching the peak temperature of post-impact metamorphism sulfur is liberated from adjacent troilite, which migrates into the metal along structural defects. Diffusion homogenizes the previous submicron cloudy zone texture. C) During subsequent cooling sulfur reacts with metal to form pyrrhotite amongst taenite/tetrataenite and Cu metal. Fast cooling transforms homogenized taenite to martensite and then plessite texture.

given sample not all composite metal-troilite grains are equally affected, which would be expected if radiogenic metamorphism were responsible. Rather, shock wave propagation affects each mineral grain differently, generating heterogeneous degrees of shock deformation, thereby offering an explanation for the observed variability.

Given the abundance of troilite in the metal component of the composite grains in Eldee 001 (typically up to 25%), a considerable amount of sulfur must have been needed to form this texture. Therefore, it is suggested that this texture requires high transient temperatures (though still subsolidus) to develop, probably equivalent to petrologic types 5 and 6. The exact temperature experienced by the Eldee 001 sample cannot be determined because migration of sulfur into the metal led to production of more sulfur than could occur under equilibrium conditions. There are rare examples in Eldee 001 of zoned taenite overprinted by zones of troilite + Cu metal in plessite (Fig. 4B; cf. Reisner and Goldstein 2003). Thus, the duration of the secondary heating event must have been sufficiently short to partially preserve these textures.

Meaning of the Van Schmus-Wood Classification

Whether the Van Schmus-Wood classification of petrologic type represents radiogenic or post-impact metamorphism in an individual meteorite is an important question that can potentially be addressed with an understanding of the kinetics of mineral reactions and elemental diffusion. Experimental studies supply some constraints on the kinetics of silicate textural/chemical equilibration, versus those of metal-troilite assemblages. At conditions above 980 °C, experimental run durations of only 2–3 days were used by Lindsley (1983) in establishing the pyroxene thermometer (although experiments were done on powders, which react quickly due to small surface area). Other experiments conducted at 1200 °C on the Leedey L6 chondrite found that after 21 days only rare relic chondrules survived (Feldstein et al. 2001). This contrasts with the rapid diffusion rate of Ni in metal versus silicates discussed earlier, and the reported rapid rate of equilibration amongst sulfides at high temperatures compared to silicates (Barton and Skinner 1979).

The slow rate of thermal diffusion in rock may allow material in the immediate vicinity of large impact craters to remain at high temperatures for longer durations than can reasonably be undertaken experimentally. Although, because impact events cause heating within a small volume, post-impact metamorphism on asteroids is a short duration event (days to years) compared with radiogenic metamorphism (a few million years). Of course, the duration and temperature of post-impact metamorphism experienced by a given sample is dependant on the size of the heat source and thus the size of the impact.

Although thick melt sheets are not expected on asteroids (Keil et al. 1997), the hottest zones in large impact craters on asteroids are likely to be immediately adjacent to thin melt sheets that are thermally insulated beneath melt breccias, which together represent the heat source (Fig. 9). Heat migrates away from this focus of heating as the superheated melt cools and begins to crystallize, forming outwardly progressing zones of contact metamorphism where more moderate temperatures are experienced. Within a sheet of impact melt breccia there are small clasts surrounded by melt, which, when situated immediately adjacent to a melt sheet, experience the maximum possible magnitude of metamorphism for a given crater. The melting reactions described above consume a small amount of thermal energy as they progress, so the heat source needs to be large enough to supply enough energy to overstep the reaction throughout a sample. Small impact melt veinlets are clearly not large enough (otherwise we would observe zones of metamorphism around them), but there is some uncertainty as to how large the heat source needs to be to produce an observable effect (heat of fusion data are needed for the taenite-troilite melting reaction before this can be calculated). The length of time that a sample anywhere within the zone of heating remains above a petrologic grade during post-impact metamorphism is significantly longer for lower grades (consider the schematic temperature-time graphs of Fig. 9).

Almost all chondritic meteorites show some evidence of impact shock. In a study of 210 ordinary chondrites of low apparent shock grades, Rubin (2004) recorded those that contained metal-troilite melt textures of the type described here. Of 53 petrologic type 5 and 6 meteorites listed as being of S1 shock class, six (11.3%) contained mosaic-textured metal-troilite grains, suggesting melting at temperatures >~850 °C. Thus, even at such low shock grades, post-impact metamorphism still appears to be a factor. These observations, amongst others, were used to suggest that the silicate minerals in many chondrites with shock grades of S1 and S2 were subject to a period of post-impact annealing, and that this process may be capable of generating silicate textures identical to those of radiogenic metamorphism (Rubin 2004). The anomalous observation amongst the population statistics that higher shock grades are more common in the higher petrologic types (Stöffler et al. 1991) can be explained as a consequence of post-impact annealing (Rubin 2004). Furthermore, the observations that some primitive achondrites contain relict chondrules, suggests that they were generated by impact processes (Rubin 2007), because the chondrules would have completely recrystallized during million year-long radiogenic metamorphism.

The petrologic classification scheme is designed to be a non-interpretational gauge of the maximum temperature reached by metamorphism, such that petrologic type is determined purely through analysis of the mineral assemblage. As has been demonstrated, in many meteorites the metal-sulfide textures, and possibly the silicate textures in some cases, do not reflect radiogenic metamorphism, but rather post-impact metamorphism. Utilizing the knowledge

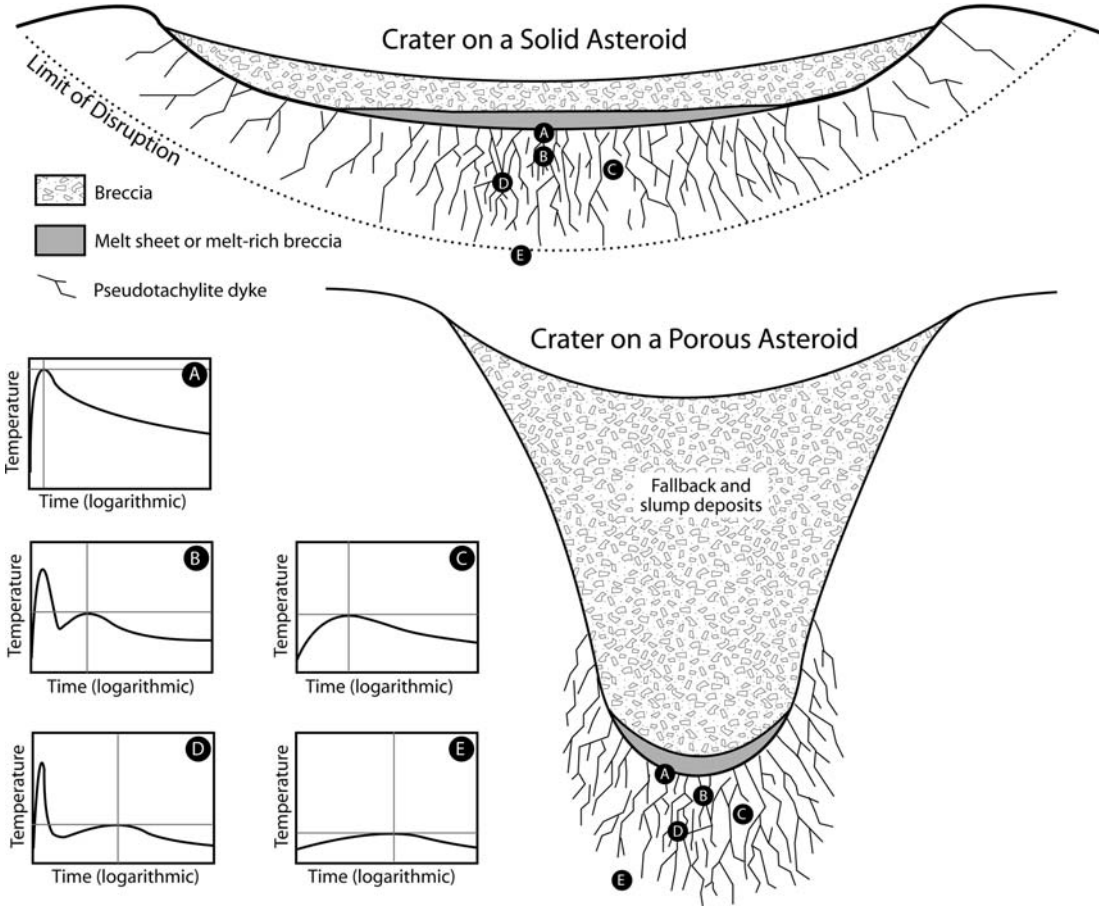

Fig. 9. Schematic cross sections of impact structures on solid and porous asteroids. Positions A through E correspond to the schematic temperature-time graphs labeled A through E, and represent heating associated with large to very large impacts. The narrow high temperature pulse in graphs A, B and D represent shock heating, causing melting, during impact within a melt sheet (A) or pseudotachylite dyke (B and D). The broader peaks represent the subsequent thermal anomaly (i.e., post-impact metamorphism) that propagates from the main center of impact heating in the vicinity of A. This contact metamorphism a much longer event than the shock heating episode due to the low thermal conductivity of silicate rocks. The duration and magnitude of heating at each position varies as a function of impact size (for example in a moderate sized structure, the textures in Hamilton might form at position A, or at position C in a very large crater), so a scale is not given in the craters or graphs. The porous asteroid sketch is based on Rubin (2005). Compare this diagram with Fig. 3 of Stöffler et al. (1991).

that metal-sulfide assemblages respond quickly to thermal changes, information can be gleaned from these as to whether a given meteorite has suffered a post-impact thermal overprint, and some constraints can be placed on the magnitude of heating. This study has found that overprinting temperatures approaching 850 °C are suggested by the observation that in composite metal-troilite grains, the metal component occasionally contains up to 50% troilite inclusions (typically <25%), with associated Cu metal possibly observed, in plessite texture (e.g., Fig. 4). In addition, where metal-troilite melt textures (mosaic textures) are developed ubiquitously throughout a sample (e.g., Figs. 1C–F, 3D), the overprinting temperature was 850–1100 °C, if no evidence of silicate melting is found. In the cases studied here, the duration of post-impact metamorphism is interpreted, based on observed relict zoned taenite + kamacite, to have been too brief for any annealing of the silicate assemblage to have occurred. Information on the duration of impact-related thermal overprint events amongst the meteorite population is critical because it determines whether the silicate assemblages were unaffected, partially affected or completely overprinted. In the latter case, the petrologic type classification would reflect the conditions of the post-impact metamorphism only.

CONCLUSIONS

The evolution of metal-troilite textures during post-impact metamorphism of chondritic meteorites has been examined. Evidence of several different processes is preserved in impact-affected meteorites. It has been recognized for some time that melt domains form during impact events on asteroids, which are characterized by immiscible emulsions of silicate melt mixed with metal and/or sulfide melt (Figs. 2A–B, 3A–B, D). These melt domains are evidence that heating during impact events tends to be

highly spatially focused and can exceed the melting point of Fe-Ni metal. This heterogeneous heat distribution must re-equilibrate over a short period of time after crater development has ceased, resulting in cooling in some domains and heating in others. Because this post-impact metamorphism occurs in the absence of a significant stress field, the resulting textures are distinctly different from those that develop during impacts.

There are two distinct metal-sulfide textures that develop during post-impact metamorphism, which reflect different thermal conditions. Firstly, melting at temperatures >~850 °C followed by in situ crystallization, generates a finely intergrown mixture of metal and troilite that lacks silicate melt spherules, with a bulk composition that is troilite-rich. In this process, zoned taenite, surviving after radiogenic metamorphism, is preferentially melted relative to kamacite, forming a Ni-rich melt that subsequently crystallizes kamacite before taenite, and produces a characteristic zoned mosaic texture (Figs. 1C–F).

Secondly, in chondrites of petrologic types 3–6, the metallic component of conjoined metal-sulfide grains contains, in many cases, numerous small inclusions of troilite, typically rimmed by taenite or tetrataenite, amongst plessite (Figs. 4A and B). These inclusions are interpreted to have formed through diffusion of sulfur from troilite into metal at high temperatures (though still subsolidus), possibly along impact-induced structural defects, which allowed subsequent formation of troilite within the metal during retrograde cooling. This texture is distinctly different to that produced by partial melting of composite metal-sulfide grains.

The much faster reaction kinetics of the metal-troilite assemblage relative to the silicate assemblage means that the former tends to equilibrate during even short thermal events, whereas the latter may show variable effects depending on the duration and magnitude of heating. In all samples studied, the duration of post-impact metamorphism was too short for significant annealing of the silicate assemblage, as evidenced by the partial preservation of zoned taenite + kamacite textures that developed during cooling from peak radiogenic metamorphism. In this way, textures developed in composite metal-troilite grains can be used to approximate the magnitude and duration of maximum heating.

Acknowledgments—The author would like to gratefully acknowledge the Schmidt family for permission to collect meteorites on their property. Roberto Weinberg is thanked for useful discussions. Dermot Henry and Bill Birch at Museum Victoria are gratefully thanked for the loan of the Hamilton meteorite and several others. Colin MacRae from CSIRO is thanked for assistance with electron microprobe work. Ed Scott, Alan Rubin, Dante Lauretta, Claude Perron, and an anonymous reviewer are thanked for their comments, which helped to significantly improve this paper. Funding for this research was provided by a Monash Fellowship to the author.

Editorial Handling—Dr. Edward Scott

REFERENCES

Barton P. B. and Skinner B. J. 1979. Sulfide mineral stabilities. In *Geochemistry of hydrothermal ore deposits*, edited by H. L. Barnes. New York: Wiley Interscience. pp. 278–403.

Bennett M. E. III and McSween H. Y. Jr. 1996. Shock features in iron-nickel metal and troilite of L-group ordinary chondrites. *Meteoritics & Planetary Science* 31:255–264.

Bogard D. D., Garrison D. H., Norman M., Scott E. R. D., and Keil K. 1995. Impact ages of meteorites: A synthesis. *Meteoritics & Planetary Science* 30:244–268.

Chennaoui Aoudjehane H., El Goresy A., and Jambon A. 2007. The assemblage native copper, cobaltian kamacite, and troilite in ordinary chondrites: Dissociation products not related to a shock event (abstract). *Meteoritics & Planetary Science* 42:A29.

Connolly H. C. Jr., Zipfel J., Grossman J. N., Folco L., Smith C., Jones R. H., Righter K., Zolensky M., Russell S. S., Benedix G. K., Yamaguchi A., and Cohen B. A. 2006. The Meteoritical Bulletin. *Meteoritics & Planetary Science* 41:1383–1418.

El Goresy A. 2006. Native copper in FeNi metal and the assemblage chromite plagioclase in ordinary chondrites: Discarded as shock parameters (abstract). *Meteoritics & Planetary Science* 41:A204.

Feldstein S. N., Jones R. H., and Papike J. J. 2001. Disequilibrium partial melting experiments on the Leedey L6 chondrite: Textural controls on melting processes. *Meteoritics & Planetary Science* 36:1421–1441.

Folco L., Bland P. A., D'Orazio M., Franchi I. A., Kelley S. P., and Rocchi S. 2004. Extensive impact melting on the H-chondrite parent asteroid during the cataclysmic bombardment of the early solar system: Evidence from the achondritic meteorite Dar al Gani 896. *Geochimica et Cosmochimica Acta* 68:2379–2397.

Hansen M. 1958. *Constitution of binary alloys*. New York: McGraw-Hill. 1305 p.

Holland T. J. B. and Powell R. 1998. An internally consistent thermodynamic dataset for phases of petrological interest. *Journal of Metamorphic Geology* 16:309–344.

Hopfe W. D. and Goldstein J. I. 2001. The metallographic cooling rate method revised: Application to iron meteorites and mesosiderites. *Meteoritics & Planetary Science* 36:135–154.

Hutchison R. and Bevan A. W. R. 1983. Conditions and time of chondrule accretion. In *Chondrules and their origins*, edited by A. E. King. Houston: Lunar and Planetary Insitute. pp. 1162–1179.

Hutchison R., Williams I. P., and Russell S. S. 2001. Theories of planetary formation: Constraints from the study of meteorites. *Philosophical Transactions of The Royal Society of London A* 359:2077–2091.

Jurewicz A. J. G., Mittlefehldt D. W., and Jones J. H. 1995. Experimental partial melting of the St. Severin (LL) and Lost City (H) chondrites. *Geochimica et Cosmochimica Acta* 59:391–408.

Keil K., Stöffler D., Love S. G., and Scott E. R. D. 1997. Constraints on the role of impact heating and melting in asteroids. *Meteoritics & Planetary Science* 32:349–363.

Kessel R., Beckett J. R., and Stolper E. M. 2007. The thermal history of equilibrated ordinary chondrites and the relationship between textural maturity and temperature. *Geochimica et Cosmochimica Acta* 71:1855–1881.

Kubaschewski O. 1982. *Iron: Binary phase diagrams*. Berlin: Springer-Verlag. 185 p.

Kullerud G. and Yund R. A. 1962. The Ni-S system and related minerals. *Journal of Petrology* 3:126–175.

Lauretta D. S., Lodders K., Fegley B. J., and Kremser D. T. 1997. The origin of sulfide-rimmed metal grains in ordinary chondrites. *Earth and Planetary Science Letters* 151:289–301.

Lindsley D. H. 1983. Pyroxene thermometry. *American Mineralogist* 68:477–493.

Mavrogenes J. A., MacIntosh I. W., and Ellis D. J. 2001. Partial melting of the Broken Hill Galena-Sphalerite ore—Experimental studies in the system PbS-FeS-ZnS-(Ag_2S). *Economic Geology* 96:205–210.

McCoy T. J., Keil K., Muenow D. W., and Wilson L. 1997. Partial melting and melt migration in the acapulcoite-lodranite parent body. *Geochimica et Cosmochimica Acta* 61:639–650.

McSween H. Y., Jr., Ghosh A., Grimm R. E., Wilson L., and Young E. D. 2002. Thermal evolution models of asteroids. In *Asteroids III*, edited by Bottke W. F., Cellino A., Paolicchi P., and Binzel R. P. Tucson, Arizona: The University of Arizona Press. pp. 559–571.

Melosh H. J. and Ivanov B. A. 1999. Impact crater collapse. *Annual Reviews of Earth and Planetary Science* 27:385–415.

Mittlefehldt D. W. and Lindstrom M. M. 2001. Petrology and geochemistry of Patuxent Range 91501, a clast-poor impact melt from the L-chondrite parent body and Lewis Cliff 88663, an L7 chondrite. *Meteoritics & Planetary Science* 36:439–457.

Monteux J., Coltice C., Dubuffet F., and Ricard Y. 2007. Thermo-mechanical adjustment after impacts during planetary growth. *Geophysical Research Letters* 34:L24201.

Petry C., Chakraborty S., and Palme H. 2004. Experimental determination of Ni diffusion coefficients in olivine and their dependence on temperature, composition, oxygen fugacity, and crystallographic orientation. *Geochimica et Cosmochimica Acta* 68:4179–4188.

Polk D. E. and Giessen B. C. 1978. Overview of principles and applications. In *Metallic glasses*, Metals Park, Ohio: American Society for Metals. pp. 1–35.

Reisner R. J. and Goldstein J. I. 2003. Ordinary chondrite metallography: Part 2. Formation of zoned and unzoned metal particles in relatively unshocked H, L, and LL chondrites. *Meteoritics & Planetary Science* 38:1679–1696.

Rubin A. E. 1990. Kamacite and olivine in ordinary chondrites: Intergroup and intragroup relationships. *Geochimica et Cosmochimica Acta* 54:1217–1232.

Rubin A. E. 1994. Metallic copper in ordinary chondrites. *Meteoritics* 29:93–98.

Rubin A. E. 2002. Smyer H-chondrite impact-melt breccia and evidence for sulfur vaporization. *Geochimica et Cosmochimica Acta* 66:699–711.

Rubin A. E. 2004. Post-shock annealing and post-annealing shock in equilibrated ordinary chondrites: Implications for the thermal and shock histories of chondritic asteroids. *Geochimica et Cosmochimica Acta* 68:673–689.

Rubin A. E. 2005. What heated the asteroids? *Scientific American* 292:80–87.

Rubin A. E. 2007. Petrogenesis of acapulcoites and lodranites: A shock melting model. *Geochimica et Cosmochimica Acta* 71: 2383–2401.

Rushmer T., Petford N., Humayun M., and Campbell A. J. 2005. Fe-liquid segregation in deforming planetesimals: Coupling core-forming compositions with transport phenomena. *Earth and Planetary Science Letters* 239:185–202.

Saikumar V. and Goldstein J. I. 1988. An evaluation of the methods to determine the cooling rates of iron meteorites. *Geochimica et Cosmochimica Acta* 52:715–726.

Scott E. R. D. 1982. Origin of rapidly solidified metal-troilite grains in chondrites and iron meteorites. *Geochimica et Cosmochimica Acta* 46:813–823.

Slater-Reynolds V. and McSween H. Y. 2005. Peak metamorphic temperatures in type 6 ordinary chondrites: An evaluation of pyroxene and plagioclase geothermometry. *Meteoritics & Planetary Science* 40:745–754.

Sommer F. 1985. Metallic glass forming ability. In *Rapidly quenched metals*, edited by S. Steeb and H. Warlimont. Amsterdam: Elsevier. pp. 153–161.

Sparks H. A. and Mavrogenes J. A. 2005. Sulfide melt inclusions as evidence for the existence of a sulfide partial melt at Broken Hill, Australia. *Economic Geology* 100:773–779.

Stöffler D., Keil K., and Scott E. R. D. 1991. Shock metamorphism of ordinary chondrites. *Geochimica et Cosmochimica Acta* 55: 3845–3867.

Tomkins A. G. and Mavrogenes J. A. 2002. Mobilization of gold as a polymetallic melt during pelite anatexis at the Challenger deposit, South Australia: A metamorphosed Archean gold deposit. *Economic Geology* 97:1249–1271.

Tomkins A. G., Pattison D. R. M., and Frost B. R. 2007. On the initiation of metamorphic sulfide anatexis. *Journal of Petrology* 48:511–535.

Toulmin P. I. and Barton J. 1964. A thermodynamic study of pyrite and pyrrhotite. *Geochimica et Cosmochimica Acta* 56:227–243.

Trieloff M., Jessberger E. K., Herrwerth I., Hopp J., Fieni C., Ghelis M., Bourot-Denise M., and Pellas P. 2003. Structure and thermal history of the H-chondrite parent asteroid revealed by thermochronometry. *Nature* 422:502–506.

Van der Bogert C. H., Schultz P. H., and Spray J. G. 2003. Impact-induced frictional melting in ordinary chondrites: A mechanism for deformation, darkening, and vein formation. *Meteoritics & Planetary Science* 38:1521–1531.

Van Schmus W. R. and Wood J. A. 1967. A chemical-petrologic classification for the chondritic meteorites. *Geochimica et Cosmochimica Acta* 31:747–765.

Villars P., Prince A., and Okamoto H. 1995. *Handbook of ternary alloy phase diagrams. Cu-Mg-Si to Ga-Hg-Te*. ASM International.

Wood J. A. 1967. Chondrites: Their metallic minerals, thermal histories and parent bodies. *Icarus* 6:1–49.